Journal of Materials Processing Technology, 270, , 2019, 1-7

Joining of metals and polymers using powder metallurgy with laser irradiation

Seung-Gwang Kim*, Asuka Suzuki, Naoki Takata, and Makoto Kobashi

Department of Materials Process Engineering, Graduate School of Engineering, Nagoya University, Furo-cho, Chikusa-ku, Nagoya 464-8603, Japan

*Corresponding author
Seung-Gwang Kim
E-mail address: kim.seung.gwang@d.mbox.nagoya-u.ac.jp

Abstract

Porous layer on an aluminum alloy (A5052) sheet for joining with a Polyamide-6 (PA6) sheets was synthesized using combustion reactions among Al, Ti, and C powders. The laser was irradiated on the bedded powder blend of Al, Ti and C to induces the combustion reactions. The porous layer consists of a number of particle-shaped protrusions. Phase identification and microstructural observation of the cross-sectioned porous layer showed that the protrusions consisting of α-Al, TiC and Al_3Ti phases, bonded well with the Al sheet. Single lap joints with PA6 and Al sheets via the porous layer were fabricated using a hydraulic hot press; PA6 infiltrated into the gaps among the particle-shaped protrusions. Fractography analysis indicated that the particle-shaped protrusions well interlocked with PA6, which resulted in a high-joint strength along with high reliability.

Keywords:

Metal/polymer joining; mechanical interlocking;
laser processing; mechanical properties; fractography

1. Introduction

Joining dissimilar materials like metals and polymers are one of the important technologies for automobile and aerospace industries. Martinsen et al. (2015) reviewed various methods in joining dissimilar materials. Adhesives and mechanical fasteners are being widely used to join metals and polymers. There are several disadvantages associated with these methods. In the case of mechanical fastening, local damage to the joined materials and galvanic corrosion are some of the potential draw-backs. Adhesive bonding requires extensive surface treatment of any adhesives, extra curing time. Tomita et al. (2017) reported that adhesion strength of structural adhesive degrades in high temperature and high humidity conditions. Alternative joining technologies are required to overcome these problems.

Various methods were proposed to form dimples on the metal surface for joining with polymers by mechanical interlocking. The mechanical interlocking acts by infiltrating the polymer into the dimples formed on the metal surface and interlocking with each other. Rodriguez-Vidal et al. (2018) generated micro-pattern on a steel surface by laser radiation and fabricated metal/polymer joints using the laser source. The metal parts without micro-pattern were joined and the joint strength increased substantially after micro-pattern was adopted. Nielsen et al. (2010) and Taki et al. (2016) utilized laser ablation technique to modify the surface of a stainless steel and an aluminum alloy, respectively. Injection molding was used to fabricated metal/polymer joints. Yeh and Hsu (2016) used ultrasonic welding to join a polymer and a laser-structured aluminum alloy. Roesner et al. (2011) modified the surface of a stainless steel with laser ablation technique and fabricated metal/polymer joints by using the laser transmission joining and the induction joining technologies. Lucchetta et al. (2011) modified an aluminum alloy surface by shot peening and metal/polymer joints were fabricated using injection molding. Kajihara et al. (2018) fabricated metal/polymer joints by injection molding after modifying the surface of aluminum alloy by sand blasting. The blasting and molding conditions were optimized for high joint strength. Goushegir et al. (2014) fabricated metal/carbon-fiber reinforced polymer joints with friction spot joining technology. The joint strength increased after metal part was sand blasted. Kimura et al. (2016) and Kleffel and Drummer (2017) modified an aluminum alloy surface by chemical process and metal/polymer joints were fabricated using injection molding.

These studies demonstrated the potential to fabricate metal/polymer hybrid structure by adopting mechanical interlocking.

Suzuki et al. (2018) proposed a joining method between metals and polymers using an “interpenetrating phase layer”. Open-cell porous-structured layer was formed on a metal substrate, and then pores were infiltrated by a polymer, resulting in the formation of a composite layer at the interface between metal and polymer. A high bonding strength can be achieved in all directions due to the 3D interlocking of the interpenetrating phase layer. However, Suzuki et al. (2018) fabricated the porous layer by powder sintering while applying pressure at high temperature. A more practical processing method to produce the porous layer is required.

One of the potential routes to produce the porous layer on the metal substrates is an additive manufacturing technology applied to the metal surface. Kobashi et al. (2010) fabricated porous Al-Ti intermetallic composites through combustion foaming process with aluminum and titanium powders. The combustion reaction of Al-Ti enhances a foaming of liquid metals, resulting in the porous-structured metals. Omura et al. (2002) demonstrated the porous structure fabricated using a mixed elemental powder of Al, Ti and C through Al-Ti and Ti-C exothermic reactions. These results open an opportunity to produce the porous layer additively fabricated on the metal surface utilizing a mixed elemental powder. However, when the substrate consists of Al-based alloys, the substrate is inevitably melted by totally heating. In the present study, focusing on the laser irradiation process for local heating without melting the substrate, an attempt was made to additively fabricate the porous layer on the Al sheet (A5052) by laser-induced combustion synthesis on the bedded powder blend layer of Al, Ti and C elements for joining Polyamide-6 (PA6) sheet. The formed porous layer was characterized in terms of its morphology, microstructure and phase composition. The A5052/PA6 joints were fabricated by using a hydraulic hot press machine. The mechanical properties of A5052/PA6 joints formed via the porous layer with various structures were studied by lap shear tests and fractography. These results were utilized to discuss on the possibility of the joining process.

2. Materials and methods

Al powder (99.99% purity, particle size <45 μm), Ti powder (99.9% purity,

particle size <45 μm) (Koujundo Chemical Lab. Co., Ltd.) and C powder (98% purity, average size of 5 nm) (Lion Specialty Chemicals Co., Ltd.) were used to prepare three types of starting powders, namely Al powder, Al-Ti powder blend (molar ratio of Al:Ti = 1:1), and Al-Ti-C powder blend (molar ratio of Al:Ti:C = 1:1:1). Each type of powder was stacked in a rectangle form with dimensions of 15 mm × 5 mm × 50 μm (length × width × height) on an A5052 Al alloy substrate (20 mm × 50 mm × 1 mm). After stacking the starting powders, a pulsed diode laser beam (wavelength: 970 nm, pulse frequency rate: 1000Hz, pulse length: 700 μs, laser beam diameter at work plane: 1.2 mm) was irradiated onto the bedded powder. The average laser power and scanning speed were controlled at 400 W and 40 mm/s, respectively. The laser scanning length was 10 mm. After the laser irradiation, the Al alloy substrate was cleaned by ultrasonic wave in water to remove unreacted powders around the formed layer. The porous layer preparation process is schematically illustrated in Fig. 1. Laser irradiating process and after ultrasonic cleaning are represented in Fig .1(A) and (B), respectively.

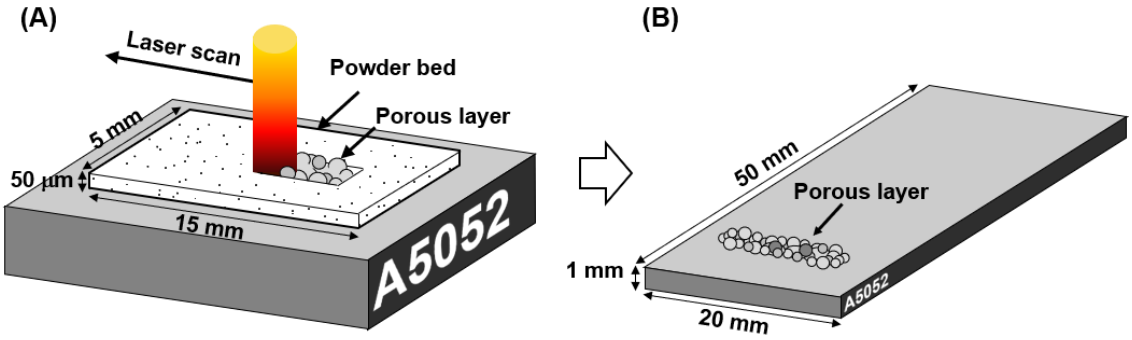

Fig. 1 Schematic illustration of the porous layer formation process on the Al alloy (A5052) substrate. (A) laser irradiating process and (B) after ultrasonic cleaning

The surface morphology and microstructure of the cross-sectioned porous layer were observed using a scanning electron microscope (SEM). The samples for cross-sectional observation were initially embedded into epoxy resin after which specimens were cross-sectioned using a cutting machine, followed by mechanical polishing with a polishing machine (Rana-30, IMT Co. Ltd.). The surfaces were polished using SiC abrasive papers (#350, #800, #1000 and #2400) and buffed using 3 μm, and 1 μm diamond suspensions and a 0.04 μm colloidal silica suspension. Energy dispersive X-

ray spectroscopy (EDS) at 20 kV was carried out to analyze elemental dispersion in the cross-sectioned samples of the porous layers formed with Al-Ti and Al-Ti-C powder blends. X-ray diffraction (XRD) measurement with Cu-Kα radiation was conducted at 40 kV and 40 mA to identify the phases constituting the porous layers formed with Al-Ti and Al-Ti-C powder blends. In the case of the porous layer fabricated with Al-Ti-C powder blend, etching was carried out with a 20% NaOH aqueous solution to investigate the dispersion morphology of synthesized products of Al-Ti-C combustion reaction (Al_3Ti, TiC). According to Vinod Kumar et al. (2005), NaOH aqueous solution dissolves Al matrix leaving behind synthesized products of Al-Ti-C combustion reaction. The etched surface was observed using the SEM.

The polymer material used for lap joint specimens was a pre-molded polyamide-6 (PA6) substrate of 20 mm × 50 mm × 3 mm (Toray Plastic Precision Co., Ltd.). Al/PA6 joints were fabricated using a hydraulic hot-pressing machine (AH-10TD, AS ONE Co., Ltd.). Fig. 2(A) schematically illustrates the fabrication process of the Al/PA6 joints. The porous layer formed Al alloy substrates were set on the hot plate of a hydraulic hot press. The hot plate was heated to 215 °C, and was later cooled down to 190 °C at a rate of 2 °C/min. A heating temperature of 215 °C was chosen as the melting point of PA6 was 225 °C. A joining pressure of 1.8 MPa was applied during the joining process. Fig. 2(B) shows the timeline history of the applied hot-sample stage temperature and joining pressure. An Al substrate in conjunction with a porous layer and an Al/PA6 joint are shown in Fig. 3. The cross-section of the Al/PA6 joint via the porous layer made from Al-Ti-C powder blend was observed using an optical microscope (ECLIPSE LV150N, Nikon Corporation) to confirm the infiltration of PA6 into the porous layer. After fabricating joint specimens, a lap shear test was conducted using a universal tensile tester (AG-1 20 kN, Shimadzu Corporation) to measure the joint strength. The joint specimens were loaded at a crosshead speed of 1 mm/min at 25 °C. Three samples of each type of Al/PA6 joints were used to estimate the ultimate lap shear force. The fracture surfaces after the lap shear tests were observed using the SEM. The joining area for each type of powder was calculated based on top view SEM image of each porous layer and image analysis software. The area where porous layers were formed was surrounded and the area was calculated. Each of 2 sample was randomly picked up and average value was calculated. The areas of Al, Al-Ti, Al-Ti-C

porous layers were 9.21, 14.4, 17.9 mm^2, respectively.

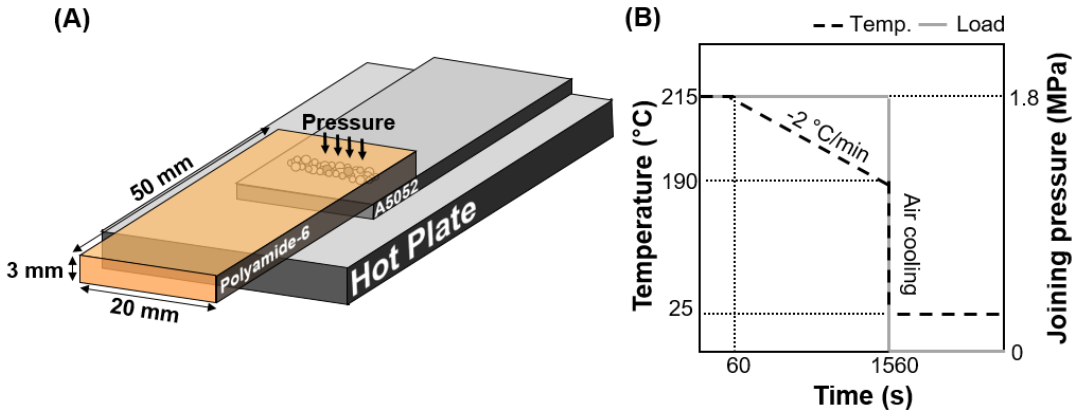

Fig. 2 (A) Schematic illustration of the Al/PA6 joint fabrication process. (B) History of the temperature of the sample stage and joining pressure.

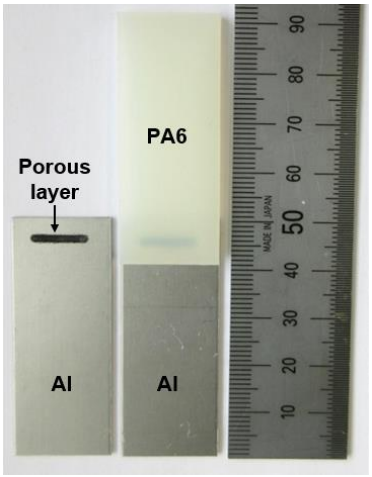

Fig. 3 Photographs of an Al substrate with a porous layer (left) and an Al/PA6 joint (right).

3. Results

3.1 Characteristics of the porous layers

Fig. 4 shows the representative SEM images of each formed porous layers. When pure Al powder used, particle-shaped protrusions were formed on the Al alloy substrate. In the corresponding high-magnification top view image, the surface was found to be smooth. A homogeneous microstructure and well-bonded boundary between the particle-shaped protrusion were observed as shown in the corresponding cross-sectional image.

In the case of using Al-Ti powder blend, a dense layer was formed as shown in the low-magnification top view image. Moreover, as indicated by the white arrows, groove-like features were formed on the dense layer. The high-magnification top view image of the structure surface indicated the presence of small dimples. An inhomogeneous microstructure and well-bonded boundary between the dense layer and Al substrate were observed in the corresponding cross-sectional image.

It was observed in the low-magnification top view image of the porous layer formed with Al-Ti-C powder blend that the layer composed of many particle-shaped protrusions. It was observed from the high-magnification image that the particle-shaped protrusion has rough surface. The cross-sectional image of the structure indicated that fine particles (brighter contrast) dispersed in the particle-shaped protrusion. The fine particles were distributed not only in the particle-shaped protrusions, but also in the Al alloy substrate, indicating that the particle-shaped protrusions are strongly bonded to the substrate.

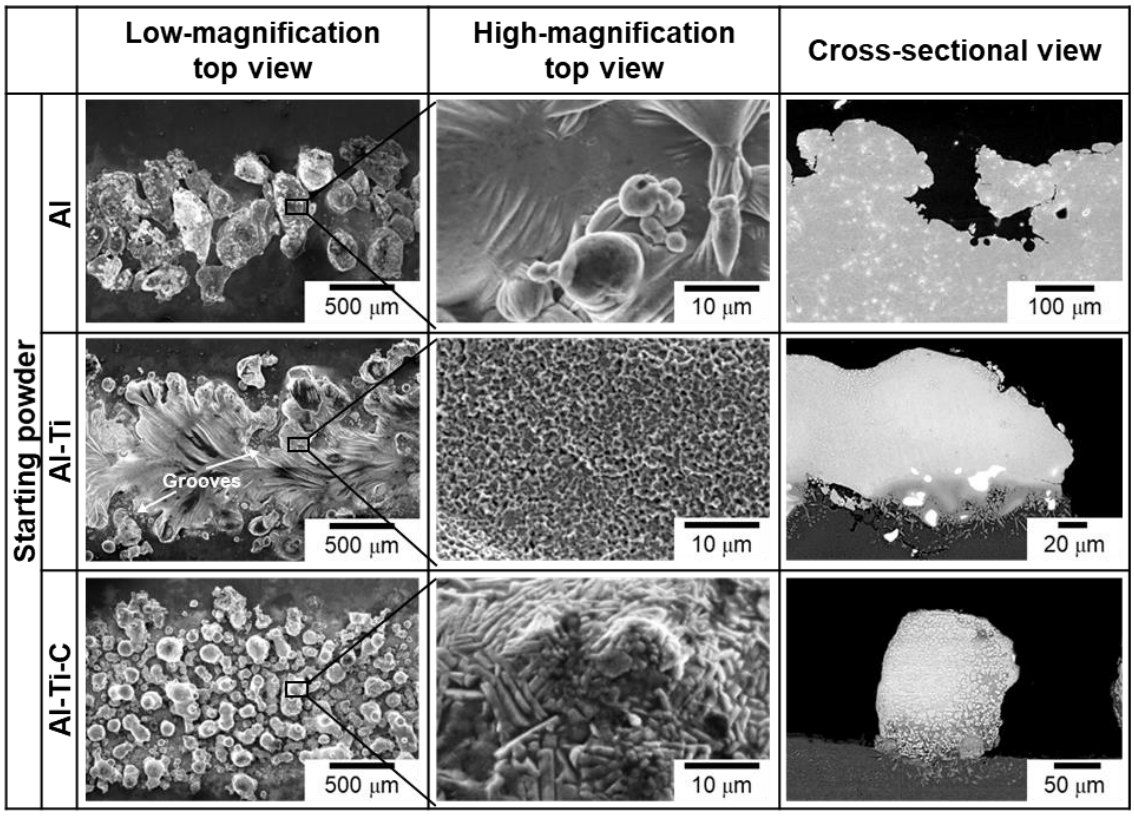

Fig. 4 Low- and high-magnification top view, and cross-sectional view of the porous layers

The XRD results of the porous layers formed with Al-Ti and Al-Ti-C powder blends are depicted in Fig. 5. Kobashi et al. (2013) reported that the final products of the combustion synthesis reaction are Al-Ti intermetallic compounds in the case of the Al-Ti powder blend. Al-TiC composite was the final product in the case of Al-Ti-C powder blend, which was reported by Omura et al. (2002). As shown in Fig. 5, in the porous layer formed with Al-Ti powder blend, various intermetallic compounds (Al_3Ti, AlTi and $AlTi_3$), and α-Ti were detected. TiN peaks were observed, which may be formed by the reaction between Ti and N_2 present in air. Al_3Ti, α-Al, and TiC, were detected in the porous layer formed with Al-Ti-C powder blend. Kβ peaks of α-Al were detected in both cases.

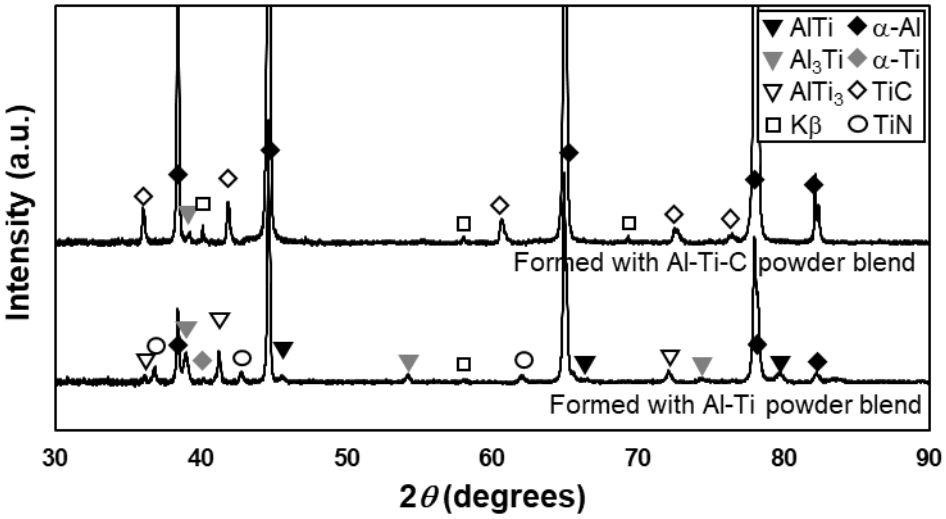

Fig. 5 X-ray diffraction patterns of the porous layers formed with different powder blends

The SEM images obtained in back scattered electron (BSE) mode and EDS element mapping results of the porous layers formed with Al-Ti and Al-Ti-C powder blends are shown in Fig. 6 and 7, respectively. In the case of the porous layer formed with Al-Ti powder blend shown in **Fig. 6**, the phase with the brightest contrast near the substrate is unreacted α-Ti because Ti element is only detected. α-Ti phase is surrounded by relatively Al-rich Al-Ti intermetallic compounds, which is Al_3Ti phase judged from XRD profile. In the region above α-Ti and Al_3Ti, relatively Ti-rich intermetallic compounds ($AlTi_3$, AlTi) were observed. The porous layer formed with Al-Ti powder blend consists of several layer with various Al-Ti intermetallic compounds

and α-Ti. The microstructure seen in the middle region of porous layer formed with Al-Ti-C powder blend indicated in **Fig.7(A)** has two phases. The brightest contrast shows TiC phase since Ti and C are detected. TiC phase was surrounded by Al-Ti phase which indicates Al_3Ti phase judged from XRD results. Near substrate indicated if **Fig.7 (B)**, α-Al phase (the darkest contrast) was observed in addition to Al_3Ti and TiC phases. The porous layer formed with Al-Ti-C powder blend is composed of the TiC, Al_3Ti and Al phases.

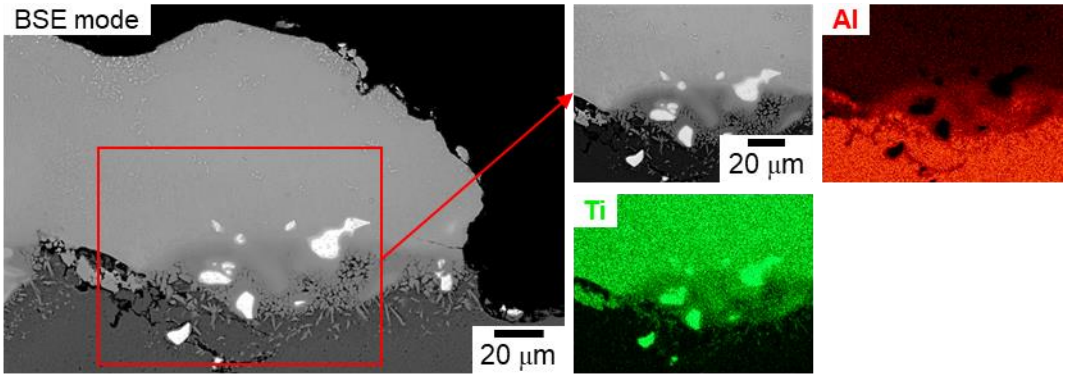

Fig. 6 EDS elemental mapping of the porous layer formed with Al-Ti powder blend

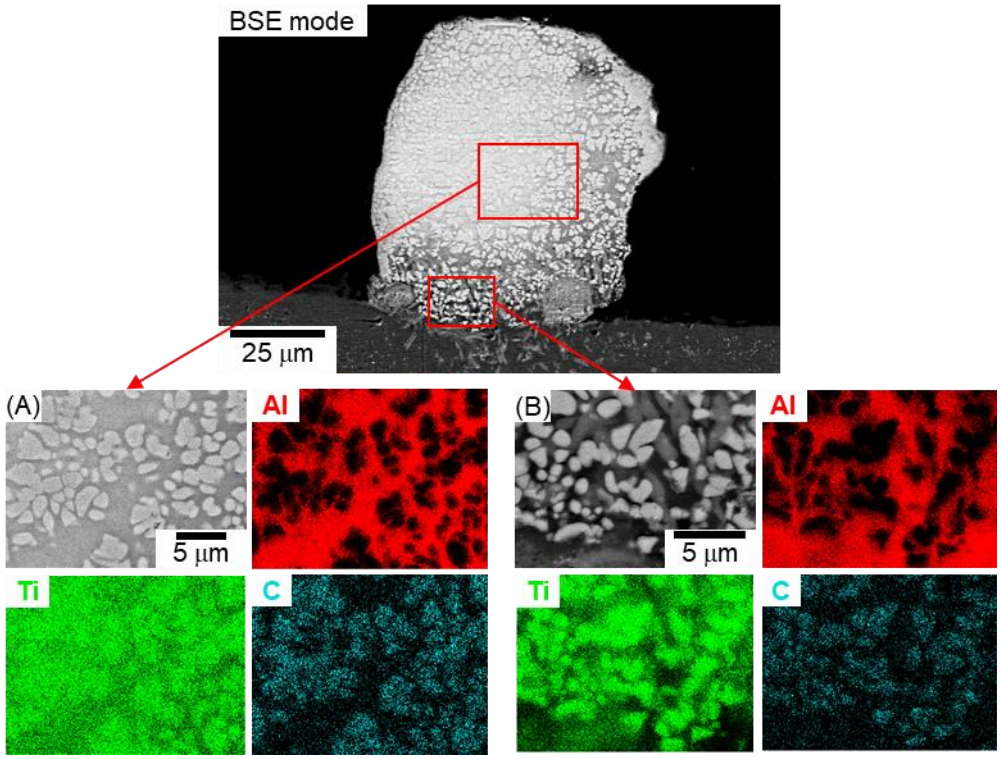

Fig. 7 EDS elemental mapping of the porous layer formed with Al-Ti-C powder blend. (A) middle region and (B) near substrate region.

SEM images of the etched particle-shaped protrusions in the porous layer formed with Al-Ti-C powder blend is shown in Fig. 8. According to the low-magnification image (Fig. 8 (A)), a particle-shape was still retained. The high-magnification image (Fig. 8 (B)) revealed that the etched protrusion exhibited a porous structure. In other words, synthesized products were remaining and connected to each other to form a skeleton of the particle-shaped protrusions.

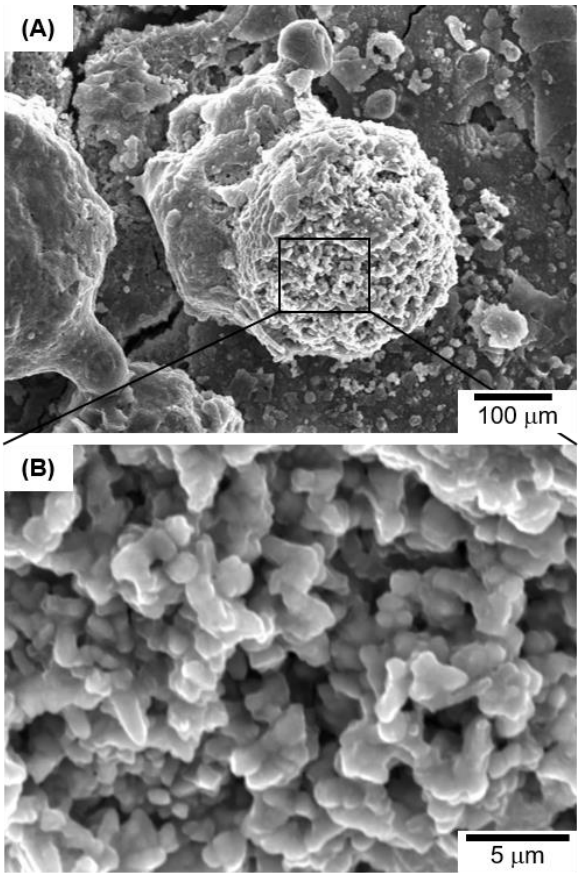

Fig. 8 Etched particle-shaped protrusion in the porous layer formed with Al-Ti-C powder blend. (A) low- and (B) high-magnification view.

3.2 Properties of Al/PA6 joints

Fig. 9 shows the cross-sectional image of a joint sample fabricated via the porous layer formed with Al-Ti-C powder blend observed using an optical microscope.

No gaps were found in the polymer/metal interface at this magnification. It is confirmed that the PA6 and Al sheet are well joined via the porous layer.

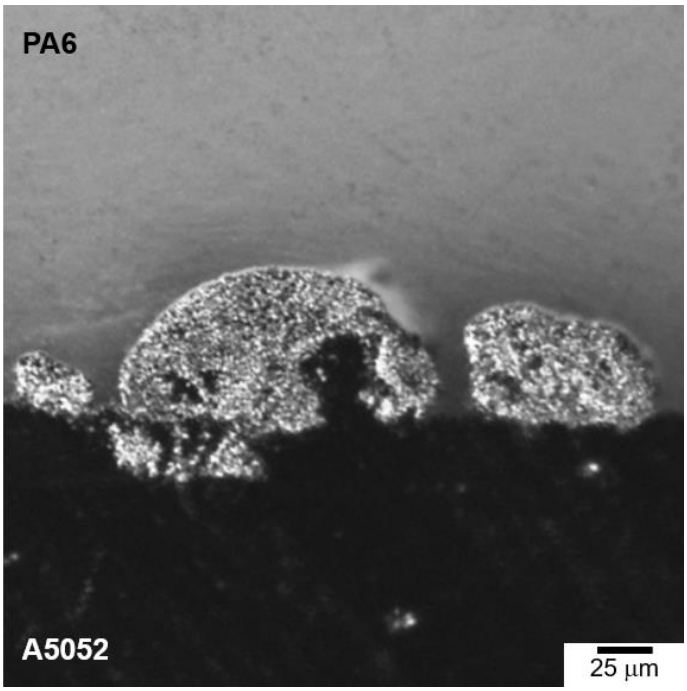

Fig. 9 Optical micrograph of the cross-section of an Al/PA6 joint

Fig. 10 (a) shows the representative lap shear force-stroke curves of Al/PA6 joints fabricated via porous layers formed with Al powder, Al-Ti and Al-Ti-C powder blends. The ultimate lap shear forces were estimated from the lap shear force-stroke curves and the average values of three test runs for each joint were calculated; the results are shown in Fig. 10 (b). The error bars show the maximum and minimum values obtained from three samples. The Al/PA6 joint fabricated via the porous layer formed with Al-Ti-C powder blend showed the highest average value of the ultimate lap shear force and the lowest difference between the maximum and minimum values of the lap shear force. These results imply that the joint fabricated via the porous layer formed with Al-Ti-C powder blend shows very strong and reliable mechanical properties.

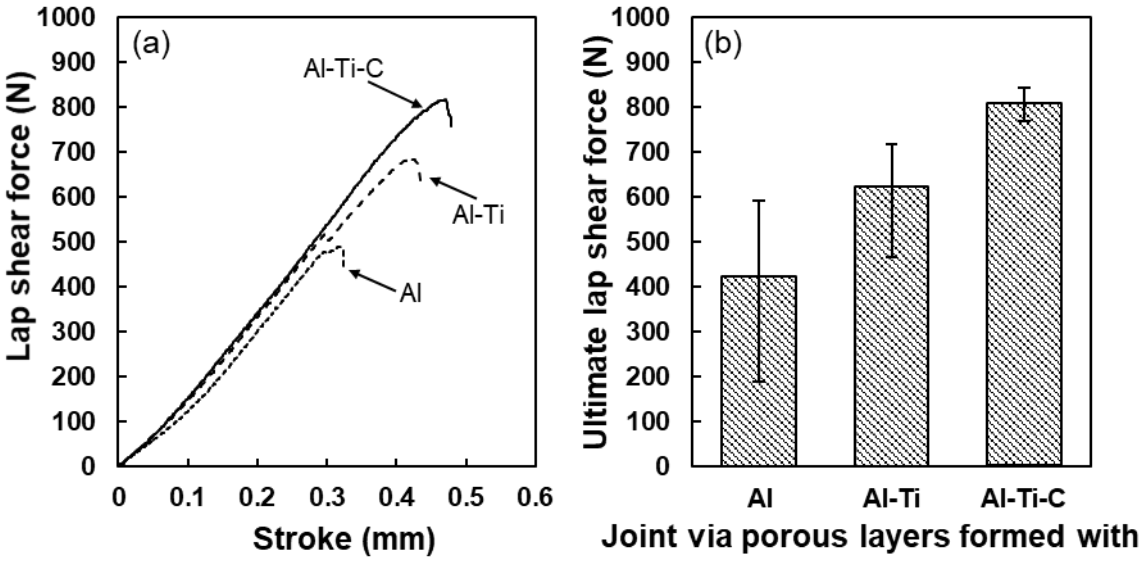

Fig. 10. (a) Lap shear force-stroke curves and (b) ultimate lap shear force of Al/PA6 joints fabricated via different porous layers. Error bar shows the maximum and minimum values obtained from three samples.

The SEM images of the porous layers before and after tensile testing are shown in Fig. 11. In the case of the porous layer formed with Al powder, most of the particle-shaped protrusions fractured after the lap shear test. Moreover, the remaining protrusions deformed severely (indicated by white arrows). PA6 was not observed in the fracture surface, which indicates interface peeling. In the fracture surface of the porous layer formed with Al-Ti powder blend, it was found that the dense layer was retained and remaining PA6 (indicated by white arrows) was observed after the lap shear test. The location of the remaining PA6 corresponds to that of the grooves formed on the porous layer (indicated by black arrows). In the case of the porous layer formed with Al-Ti-C powder blend, remaining PA6 (indicated by black arrow) was found among the remaining particle-shaped protrusions.

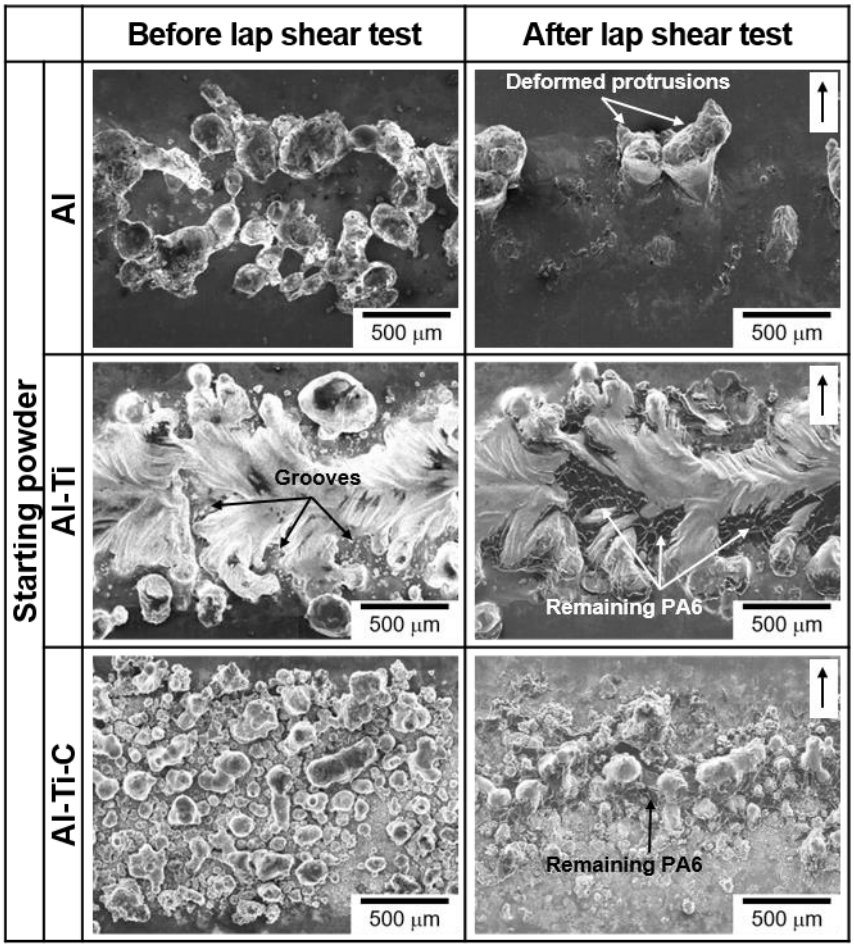

Fig. 11 SEM images of the porous layer before and after lap shear test (Black arrow in white box shows the direction of the applied shear force)

4. Discussion

4.1 Formation mechanism of porous layers

The structure of the porous layer formed with Al powder consisted of particle-shaped protrusions. Li et al. (2012) reported that, during laser radiation on metal powder, the so-called balling phenomenon occurs under specific laser conditions due to the poor wettability and shrinking tendency of the molten metal, which decreases its surface energy. The particle-shaped protrusions were formed because of the balling phenomenon of Al powder.

When Al-Ti powder blend used, a dense layer was formed and various Al-Ti intermetallic compounds were synthesized. Yang et al. (2018) measured the wettability between the molten AgCuTi metal and a SiC substrate by sessile drop method. The wettability improved with the increase of Ti content in the molten metal, which was

caused by the chemical reaction between the Si and Ti elements. Therefore, the formation of the dense layer is attributed to the reaction between Al in the substrate and Ti elements. In fact, Al-Ti intermetallic compounds are observed not only inside the dense layer but also at the dense layer/Al substrate. Kobashi et al. (2013) synthesized Al-Ti intermetallic compounds with an Al-Ti powder blend (1:1 molar ratio) in an induction furnace. When the temperature of the Al-Ti powder blend reached the vicinity of the melting point of Al, combustion reaction was initiated and Al-Ti intermetallic compounds were synthesized. In the present study, it is considered that the used laser can supply enough heat to melt the Al powder and induce a combustion synthesis reaction between Al and Ti; this discussion is further supported by the fact that melting of Al was observed when Al powder was used. Unreacted α-Ti phase was observed near the substrate. This is because the reaction heat flows to the substrate, and the reaction is not completed. This results indicate that Al_3Ti surrounding α-Ti phase is the first product of the reaction.

The addition of C powder into the Al-Ti powder blend changed the morphology and constituent phases of the porous layer. Omura et al. (2002) studied the formation mechanism of TiC-dispersed Al matrix composites fabricated by heating Al-Ti-C powder blend in an induction furnace. When the temperature of the powder blend reached the vicinity of the melting point of Al, a solid Al-Ti intermetallic compound was produced due to the combustion synthesis reaction between Al and Ti. According to the calculated adiabatic combustion temperature, it exceeds the melting point of the AlTi intermetallic compound. Under such conditions, combustion synthesis can occur between C and Ti in Al-Ti liquid solution, and a TiC-dispersed Al matrix composite is formed. In the particle-shaped protrusion, a TiC and Al_3Ti phases were formed in Al phase. In this case, the melting of Al_3Ti phase compounds induces the Ti-C reaction, which releases further heat. As a result, α-Ti is completely consumed. The formation of particle-shaped protrusions may be related to the formed skeleton (Fig.8). The reason why the reaction products were not dispersed as grains but connected as a skeleton needs to be investigated.

4.2 Mechanical properties of Al/PA6 joints

In case of the Al/PA6 joint fabricated via the porous layer formed with Al

powder, most of the protrusions were fractured and remaining protrusions were severely deformed along the direction of the tensile stress (Fig. 11), which means that the particle-shaped protrusions could not resist shear forces. This result suggests that a constituent phase which gives good mechanical property is required for the porous layer.

Higher joint strength of the Al/PA6 joint fabricated via the porous layer formed with Al-Ti powder blend was caused by Al-Ti intermetallic phases in the porous layer. Ward-Close et al. (1995) reviewed the development in intermetallic-matrix composites. Al-Ti intermetallic compounds show high elastic modulus and high strength compared to pure Al. As a result, the porous layer could resist high shear force. This resistance could allow the grooves to interlock with PA6 when a shear force was applied; further, PA6 fractured instead of peeling off from the surface.

The remarkable mechanical behavior of the Al/PA6 joint fabricated via the porous layer formed with Al-Ti-C powder blend is derived from the TiC and Al_3Ti phase in the porous layer and its structural features. According to Omura et al. (2002), dispersed TiC reinforces the Al matrix and the Al-TiC composite displays a high specific strength and stiffness. Consequently, the particle-shaped protrusions were hard to be fractured and enabled PA6 to interlock with each of the protrusions. The particle-shaped protrusions were homogeneously formed along with the whole laser scanned area, resulting in the high joint strength.

The lap joint strength of the Al/PA6 joint fabricated via the porous layer formed with Al-Ti-C powder blend was about 45.1 MPa, which was the result obtained when the ultimate lap shear force (807.6 N) was divided by the surface area of the porous layer formed with Al-Ti-C powder blend (17.9 mm^2). Seong et al. (2008) carried out parametric study on the failure with bonded single-lap joints. The tensile shear strength with a unit of [N] generally do not have a linear correlation with the bonded area even when the joining conditions are same. The lap shear test is not a proper method to measure the joint strength. Although it is necessary to change the joining area or to perform a tensile strength test in the normal direction to the interface, the bonding technique developed in this study is considered to be efficient.

It is thought that the morphology of the porous layer are changed by process condition such as powder molar ratio and laser condition. The effect of process condition

on the morphology of porous layer and joint strength needs to be investigated. PA6 is semi-crystalline polymer and the crystalline property of PA6 are influenced by joining condition. The effect of joining condition on crystalline property and joint strength needs to be investigated.

5. Conclusions

- Porous layer was formed on A5052 sheet by laser irradiating on Al-Ti-C powder blend bed.
- The porous layer consisted of homogeneously distributed particle-shaped protrusions reinforced by TiC and Al_3Ti phases.
- TiC and Al_3Ti phases help the particle-shaped protrusions to resist high shear force.
- The particle-shaped protrusions formed along with the whole laser scanned area provided a lot of interlocking sites, resulting in high joint strength.

Acknowledgment

The authors are grateful to Tomohiro Maeda from Kisoh Co.,Ltd for his valuable comments and supports.

Reference

- Goushegir, S.M., Dos Santos, J.F., Amancio-Filho, S.T., 2014. Friction spot joining of aluminum AA2024/carbon-fiber reinforced poly(phenylene sulfide) composite single lap joints: microstructure and mechanical performance. Mater. Des. 54, 196-206.
- Kajihara, Y., Tamura, Y., Kimura, F., Suzuki, G., Nakura, N., Yamaguchi, E., 2018. Joining strength dependence on molding conditions and surface textures in blast-assisted metal-polymer direct joining. CIRP Ann.-Manuf. Technol. 67, 591-594.
- Kimura, F., Kadoya, S., Kajihara, Y., 2016. Effects of molding conditions on injection molded direct joining using a metal with nano-structured surface. Precis. Eng. 45, 203-208.
- Kleffel, T., Drummer, D., 2017. Investigating the suitability of roughness parameters to assess the bond strength of polymer-metal hybrid structures with mechanical adhesion. Compos. Part B 117, 20-25.
- Kobashi, M., Inoguchi, N., Kanetake, N., 2010. Effect of elemental powder blending ratio on combustion foaming behavior of porous Al-Ti intermetallics and Al_3Ti/Al composites. Intermetallics 18, 1039-1045.
- Kobashi, M., Miyake, S., Kanetake, N., 2013. Hierarchical open cellular porous TiAl manufactured by space holder process. Intermetallics 42, 32-34.
- Li, R., Liu, J., Shi, Y., Wang, L., Jiang, W., 2012. Balling behavior of stainless steel and nickel powder during selective laser melting process. Int. J. Adv. Manuf. Technol. 59, 1025-1035.
- Lucchetta, G., Marinello, F., Bariani, P.F., 2011. Aluminum sheet surface roughness correlation with adhesion in polymer metal hybrid overmolding. CIRP Ann.-Manuf. Technol. 60, 559-562.
- Martinsen, K., Hu, S.J., Carlson, B.E., 2015. Joining of dissimilar materials. CIRP Ann.-Manuf. Technol. 64, 679-699.
- Nielsen, J.B., Boll, J.V., Holm, A.H., Højsholt, R., Balling, P., 2010. Ultra-high-strength micro-mechanical interlocking by injection molding into laser-structured surfaces. Int. J. Adhes. Adhes. 30, 485-488.
- Omura, N., Kobashi, M., Choh, T., Kanetake, N., 2002. Synthesis of TiC particle reinforced aluminum composite by reactive infiltration process. The Japan Institute

of Metals and Materials 66, 1317-1324.

- Rodriguez-Vidal, E., Sanz, C., Lambarri, J., Quintana, I., 2018. Experimental investigation into metal micro-patterning by laser on polymer-metal hybrid joining. Opt. Laser Technol. 104, 73-82.
- Roesner, A., Scheik, S., Olowinsky, A., Gillner, A., Reisgen, U., Schleser, M., 2011. Laser assisted joining of plastic metal hybrids. Phys. Procedia 12, 370-377.
- Seong, M.S., Kim, T.H., Nguyen, K.H., Kweon, J.H., Choi, J.H., 2008. A parametric study on the failure of bonded single-lap joints of carbon composite and aluminum. Compos. Struct. 86, 135-145.
- Suzuki, A., Arai, Y., Takata, N., Kobashi, M., 2018. Effect of layer thickness on bonding strength of Al/epoxy resin joints via interpenetrating phase layer. J. Mater. Proc. Tech. 254, 338-345.
- Taki, K., Nakamura, S., Takayama, T., Nemoto, A., Ito, H., 2016. Direct joining of a laser-ablated metal surface and polymers by precise injection molding. Microsyst. Technol. 22, 31-38.
- Tomita, Y., Shohji, I., Koyama, S., Shimizu, S., 2017. Degradation behaviors of adhesion strength of structure adhesive for weld-bonding under high temperature and humidity conditions. Procedia Eng. 184, 231-237.
- Vinod Kumar, G.S., Murty, B.S., Chakraborty, M., 2005. Development of Al-Ti-C grain refiners and study of their grain refining efficiency on Al and Al-7Si alloy. Alloys Compd. 396, 143-150.送迎
- Ward-Close, C.M., Minor, R., Doorbar, P.J., 1995. Intermetallic-matrix composites-a review. Intermetallics 4, 217-229.
- Yang, J., Huang, J., Ye, Z., Chen, S., Ji, R., Zhao, Y., 2018. Influence of interfacial reaction on reactive wettability of molten Ag-Cu-X wt.%Ti filler metal on SiC ceramic substrate and mechanism analysis. Appl. Surf. Sci. 436, 768-778.
- Yeh, R.Y., Hsu, R.Q., 2016. Development of ultrasonic direct joining of thermoplastic to laser structured metal. Int. J. Adhes. Adhes. 65, 28-32.

Figure captions

Fig. 1 Schematic illustration of the porous layer formation process on the Al alloy (A5052) substrate. (A) laser irradiating process and (B) after ultrasonic cleaning

Fig. 2 (A) Schematic illustration of the Al/PA6 joint fabrication process. (B) History of the temperature of the sample stage and joining pressure.

Fig. 3 Photographs of an Al substrate with the porous layer (left) and an Al/PA6 joint (right).

Fig. 4 Low- and high-magnification top view, and cross-sectional view of the porous layers

Fig. 5 X-ray diffraction patterns of the porous layers formed with different powder blends

Fig. 6 EDS elemental mapping of the porous layer formed with Al-Ti powder blend

Fig. 7 EDS elemental mapping of the porous layer formed with Al-Ti-C powder blend. (A) middle region and (B) near substrate region.

Fig. 8 Etched particle-shaped protrusion in the porous layer formed with Al-TI-C powder blend. (A) low- and (B) high-magnification view.

Fig. 9 Optical micrograph of the cross-section of an Al/PA6 joint

Fig. 10 (a) Lap shear force-stroke curves and (b) ultimate lap shear force of Al/PA6 joints fabricated via different porous layers. Error bar shows the maximum and minimum values obtained from three samples.

Fig. 11 SEM images of the porous layer before and after lap shear test (Black arrow in white box shows the direction of the applied shear force)